Lattice quantum geometry controlling 118 K multigap superconductivity in heavily overdoped $CuBa_2Ca_3Cu_4O_{10+\delta}$

Gaetano Campi,[1,2,*] Massimiliano Catricalà,[1] Giuseppe Chita,[3] Luisa Barba,[3] Luchuan Shi,[4] Jianfa Zhao,[4] Changing Jin,[4,†] and Antonio Bianconi[1,2]

[1]*Institute of Crystallography, National Research Council, CNR, Via Salaria Km 29.3, 00015 Monterotondo, Rome, Italy*

[2]*Rome International Center for Materials Science Superstripes RICMASS, Via dei Sabelli 119A, 00185 Rome, Italy*

[3]*Institute of Crystallography, National Research Council, CNR, Strada Statale 14 - Km163.5, Area Science Park, 34149 Basovizza, Trieste, Italy*

[4]*Beijing National Laboratory for Condensed Matter Physics, Institute of Physics, Chinese Academy of Sciences, Beijing 100190, China*

(Received 17 April 2025; accepted 20 August 2025; published 2 September 2025)

Synchrotron x-ray diffraction has been used to study the thermal structure evolution in $CuBa_2Ca_3Cu_4O_{10+\delta}$ (Cu1234), a superconductor which exhibits a high critical temperature ($T_C \approx 118$ K), high critical current density, and large upper critical magnetic field. The lattice geometry at the nanoscale of this cuprate belongs to the class of natural heterostructures at the atomic limit, like the artificial high T_c superlattices made of interface space charge in Mott insulator units intercalated by metal units. Temperature-dependent lattice parameters reveal a distinct lattice anomaly at T_C characterized by a drop of the *c*-axis and in-plane Cu-O negative thermal expansion below T_C. These results are consistent with a multigap scenario and complex networks of multiscale configurations controlling macroscopic superconducting functions in complex perovskites. In the multigap scenario, the lattice reorganization associated with the chemical potential changes could be assigned to the opening of multiple superconducting gaps in different points of the electron momentum space. Evidence for oxygen diffusion is observed at temperatures above 200 K. We construct a phase diagram correlating temperature, the *c*/*a*-axis ratio, and in-plane Cu-O strain, identifying regions associated with gaps opening and oxygen diffusion. These findings provide insights into how lattice geometry controls superconductivity to inform the material design of advanced nanoscale superconducting artificial quantum heterostructures.

DOI: 10.1103/9x2k-rc98

I. INTRODUCTION

High-temperature superconductivity has been a subject within materials science, focusing on the synthesis of new materials with improved superconducting properties. The field has captivated researchers due to the underlying mesoscopic complex quantum matter and potential for groundbreaking applications. In recent years, complex nanostructured heavily overdoped cuprate perovskites, grown under high oxygen pressure and high-temperature conditions, have emerged as a cornerstone of research for high critical temperature superconductors [1–10]. The $CuBa_2Ca_3Cu_4O_{10+\delta}$ (Cu1234) superconducting compound, belonging to the $CuBa_2Ca_{n-1}Cu_nO_{2n+2+\delta}$ homologous series, exhibits a critical temperature, T_C, exceeding 110 K at ambient pressure, comparable to Hg-based, which holds the highest T_C among cuprates [11–14]. Furthermore, Cu1234 demonstrates superior critical current densities (J_C) at liquid nitrogen temperature, outperforming Bi-based superconductors and rivaling the widely used $YBa_2Cu_3O_{7-\delta}$ (YBCO) [15–24]. These cuprate superconductors are renowned for hosting emergent electronic phenomena, including enhanced superconductivity in the presence of multiple superconducting gaps [25–40]. It has been pointed out [32] that variations in the chemical potential at the superconducting transition temperature, T_C, resulting from the opening of superconducting gaps, become significant primarily in the case of multiband superconductivity, particularly when one of the Fermi surfaces lies near the edge of a conduction band. In such scenarios, the chemical potential experiences substantial changes between the normal and superconducting phases. This effect is especially pronounced when the chemical potential is tuned close to the band edge of a newly emerging band in the crossover regime. Here, the relative change in chemical potential exceeds that expected in the standard BCS regime, where such variation is typically negligible. This leads to a pronounced lattice anomaly driven by charge redistribution across bands with differing superconducting gaps.

Recent studies have underscored the pivotal role of lattice complexity in determining their superconducting properties [41–65]. This complexity encompasses lattice distortions proposed by Muller [47–55] and Goodenough [56–62], validated by experimental methods probing the local structure [63–65], oxygen interstitials rearrangements [42–46], strain in CuO_2 2D layers, [66–68] and negative thermal expansion around T_C [69–76]. Such lattice complexity is closely linked to nanoscale electronic phase separation [77–79]. While the evolution of lattice complexity with temperature, such as dopant oxygen interstitials, diffusion has been extensively studied in systems like $YBa_2Cu_3O_{6+\delta}$ [42,43], La_2CuO_{4+y} [44,45], and

*Contact author: gaetano.campi@cnr.it
†Contact author: Jin@iphy.ac.cn

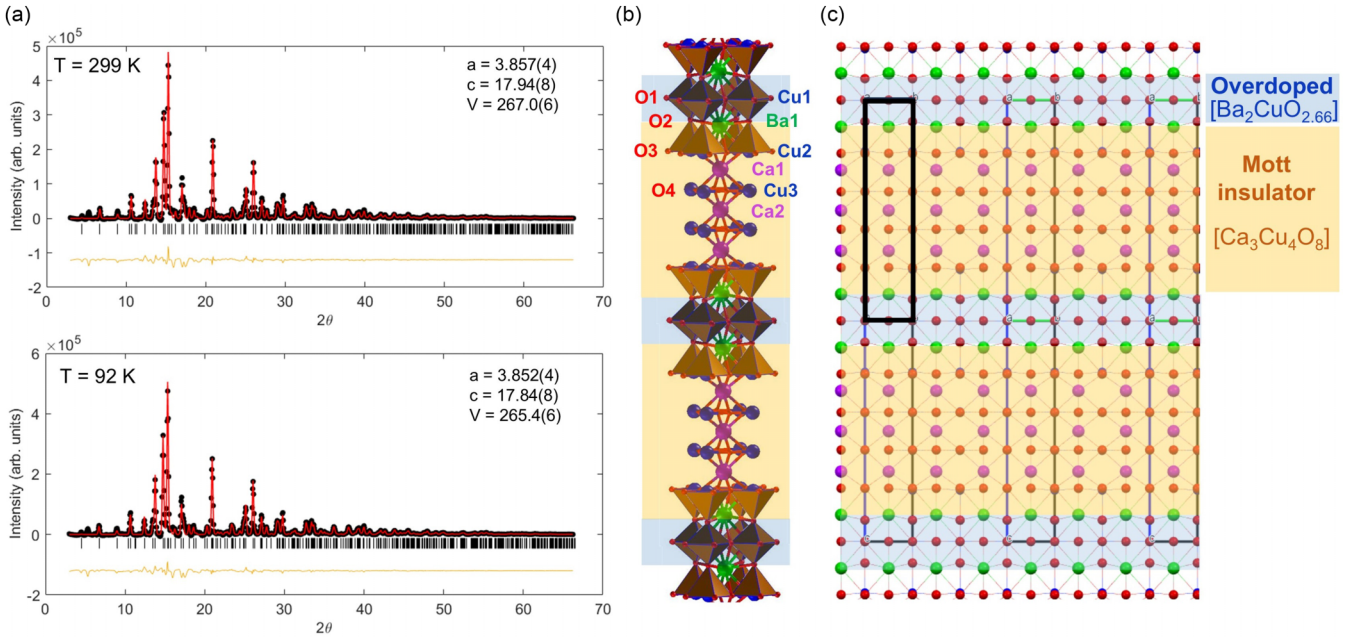

FIG. 1. (a) Rietveld refinement of the Cu1234 XRD patterns collected at T = 299 K and T = 92 K during a cooling ramp, using synchrotron radiation at ELETTRA (see methods). (b) Unit cells of Cu1234 along the c-direction with indicated atoms in the asymmetric unit. (c) View of crystalline packing highlighting the layered structure, recalling MIMI artificial nanoscale heterostructures at the atomic limit, as described in the text. The light blue and orange strips represent the overdoped $[Ba_2CuO_{2+\delta}]$ and hole-doped Mott insulator $[Ca_3Cu_4O_8]$ layers. The thick rectangle indicates the unit cell.

$HgBa_2CuO_{4+y}$ [46], analogous investigations on Cu1234 are lacking.

In this work, we explore the temperature-dependent lattice geometry of polycrystalline Cu1234 using synchrotron x-ray diffraction (XRD) across a wide temperature range. Our findings reveal a distinct lattice anomaly at T_C, characterized by a collapse of the *c*-axis and negative thermal expansion in the Cu-O plane. Additionally, we observe lattice fluctuations consistent with oxygen atom diffusion occurring above 200 K. By constructing a comprehensive phase diagram correlating temperature, lattice anisotropy, and strain, this study sheds light on how lattice reorganization drives superconducting behavior in heavily overdoped cuprates.

A key aspect of our interpretation involves the layered structure of Cu1234, which alternates between metallic and Mott insulating units. This natural architecture resembles artificial nanoscale heterostructures, akin to Mott insulator-metal interface (MIMI) systems [81–87]. Consequently, these natural and artificial superlattices provide a unique platform to investigate the interplay between distinct electronic states within CuO_2 planes, with potential implications for enhanced superconductivity. We focus on the experimental characterization of lattice quantum geometry and its changes at T_c with the aim to present robust structural evidence of lattice distortions accompanying superconductivity.

II. RESULTS AND DISCUSSION

We have studied the temperature evolution of the polycrystalline Cu1234 synthesized under high oxygen pressure and high-temperature conditions as described in [15]. The overall crystal structure of Cu1234 is typically tetragonal, in the P4/mmm space group. Rietveld refinement of Synchrotron XRD patterns collected on the XRD1 beamline at ELETTRA [88] on Cu1234 at different temperatures has been performed by using Expo2 [89] (see Methods). The XRD powder patterns collected with x-ray wavelength of 0.7 Å, alongside the Rietveld best fitted lines, at T = 299 K and at T = 92 K are shown in Fig. 1(a). We find average volumetric thermal expansion coefficients $\Delta V/V\Delta T$ of $2.2 \times 10^{-5}\,K^{-1}$ and $4.3 \times 10^{-5}\,K^{-1}$ during the cooling and heating ramps, respectively. The doubling of this coefficient in the heating ramp could be ascribed to the interstitial oxygen rearrangement, as discussed ahead. The refined chemical composition of Cu1234 agreed with data determined through neutron powder diffraction [19]. More details on the refined structural parameters at 299 K and at T = 92 K are listed in Table I.

Cu1234 is a complex, layered perovskite-like structure composed of alternating Mott insulator $[Ca_3Cu_4O_8]$ and metallic units $[Ba_2CuO_{4-y}]$ with an average valence state of copper Cu (+2.29) [19], establishing Cu1234 as a heavily overdoped layered cuprate superconductor [1–10]. The charge local redistribution has been investigated by Jarlborg *et al.* [76–79] in La-based and Hg-based cuprates, revealing that dopant-induced charges in similar systems (e.g., $HgBa_2CuO_{4+\delta}$) are predominantly localized within the $[Ba_2CuO_{4-y}]$ metallic layers, rather than uniformly distributed. This localization leads to the emergence of nanoscale phase separation, forming a natural heterostructure at the atomic limit [29], which is similar to artificial high T_c superlattices (AHTS), fostering the amplification of superconductivity by Fano-Feshbach resonance in multigap systems with relevant Rashba spin orbit coupling at the interface [81–87].

TABLE I. Fractional coordinates, x, y, z, isotropic Debye-Waller factor, U_{iso}, and occupancy, n, for each atom in the asymmetric unit of Cu1234 at room temperature, 299 K, and after the first cooling cycle at T = 92 K. We note the tendency to lower U_{iso} factors at lower temperatures, as expected, except for the O1 atoms on the basal CuO_2 planes and O3. R_p and R_{wp} values are 6.33% and 7.64% at 299 K and 6.32% and 7.62% at 92 K.

	T=299 K					T=92 K				
Atom	x	y	z	U_{iso} (Å^2)	n	x	y	z	U_{iso} (Å^2)	n
Ba1	0.5	0.5	0.1211(2)	0.0213(14)	1.000	0.5	0.5	0.1211(2)	0.0188(10)	1.000
Ca1	0.5	0.5	0.3162(6)	0.011(3)	1.000	0.5	0.5	0.3172(6)	0.013(2)	1.000
Ca2	0.5	0.5	0.5000	0.021(4)	1.000	0.5	0.5	0.5000	0.018(3)	1.000
Cu1	0.0	0.0	0.0000	0.078(6)	0.94(3)	0.0	0.0	0.0000	0.068(5)	0.94(3)
Cu2	0.0	0.0	0.2309(3)	0.0085(16)	1.000	0.0	0.0	0.2314(3)	0.0090(13)	1.000
Cu3	0.0	0.0	0.4115(3)	0.0090(18)	1.000	0.0	0.0	0.4116(3)	0.0086(14)	1.000
O1	0.0	0.5	0.0000	0.13(5)	0.55(3)	0.0	0.5	0.0000	0.13(5)	0.55(3)
O2	0.0	0.0	0.099(2)	0.018(10)	0.78(2)	0.0	0.0	0.097(2)	0.013(8)	0.78(2)
O3	0.0	0.5	0.2422(10)	0.000(4)	1.000	0.0	0.5	0.2412(10)	0.001(4)	1.000
O4	0.0	0.5	0.4145(11)	0.014(6)	1.000	0.0	0.5	0.4149(11)	0.008(5)	1.000

In our Cu1234 sample, the metallic [Ba_2CuO_{4-y}] layers exhibit an unusual compressed octahedral coordination, differentiating them from conventional cuprates. This compression lifts the $3d_{z^2-r^2}$ orbital above the $3d_{x^2-y^2}$ orbital, altering the electronic hierarchy near the Fermi level in unconventional highly doped Ba_2CuO_{4-y} [7–10,93–101]. The charge disproportionation localized at the basal CuO_2 plane is shown by unusually compressed Cu apical oxygen distances, significantly affecting orbital hybridization and promoting multiband superconductivity. Indeed, at room temperature, the estimated Cu-O bond lengths are Cu1 − O1 = 1.928 Å in-plane and Cu1 − O2 = 1.768 Å along the *c*-axis. This inverted bond-length hierarchy demonstrates that the CuO_6 octahedra are compressed like in Ba_2CuO_{4-y} contrasting sharply with standard cuprates, where the Cu-O in-plane bond is typically shorter than the Cu-O bond along the *c*-axis.

As illustrated in Fig. 1(b), Ba1 O2 Cu1 O1 sites constitute the defective overdoped [Ba_2CuO_{4-y}] normal metal (N) units with thickness W = 4.33 Å (blue thin units). Meanwhile, Cu2, Cu3, Ca1, Ca2, O3, O4 form the tick superconducting (S) units, composed of a modulation-doped stoichiometric Mott insulator [$Ca_3Cu_4O_8$] with thickness L = 13.61 Å, at low temperatures.

The geometrical parameter characterizing the MIMI heterostructures' superconducting performance is given by L/d [81–84], where L = d − W is the thickness of the metallic overdoped layer and d is the repeating unit (*c*-axis). In this Cu1234 sample, we have L/d = 0.75, that is a value falling in the predicted range for the L/d values in proximity of the top of the superconducting dome [81–87]. The structure recalling the AHTS superconducting heterostructures at the nanoscale [81–87] is depicted in Fig. 1(c).

Figure 2 illustrates the temperature-dependent structural evolution of the polycrystalline powder during cooling and heating cycles. Figure 2(a) shows colormaps of XRD intensity as a function of temperature and d-spacing for the 001 and 200 reflections, measured using an x-ray wavelength of 1.4089 Å. Gaussian fitting of these peaks across all temperatures allowed extraction of temperature evolution of unit cell parameters ***a*** and ***c***, as well as peak widths Δd_{200} and Δd_{001}. Figure 2(b) presents the temperature-dependent variations of ***a*** and ***c***, normalized to the superconducting critical temperature (T_C). Three regimes are identified. In regime (1), below T_C, the ***c***-axis sharply collapses from 17.82 Å at T_C to 17.70 Å at 92 K, accompanied by negative thermal expansion of the ***a***-axis. This behavior reflects lattice distortions, likely driven by anisotropic vibrations and CuO_6 octahedral rotations, as proposed by Purans *et al.* [73], where rotations or distortions of CuO_6 octahedra in the perovskite-type ScF_3 structure are driven by anisotropic thermal vibrations. In regime (2) between T_C and the oxygen ordering temperature ($T_O > 200$ K), the *c*-axis exhibits contraction and expansion rates (5.16×10^{-5} K^{-1}) during cooling and heating, while the ***a***-axis expands with rate 0.71×10^{-5} K^{-1} . In regime (3), above T_O, the heating ramp causes rapid expansion of the ***c***-axis from 17.89 Å at T_O to 17.94 Å at 299 K, contrasting with its stability during cooling.

This cusp is attributed to oxygen rearrangements along the *c*-axis. Figure 2(c) highlights fluctuations in lattice spacing, $\Delta d_{200}/d_{200}$ and $\Delta d_{001}/d_{001}$, across these regimes. Below T_C, fluctuations decrease sharply, stabilizing the superconducting state. Between T_C and T_O, in-plane fluctuations remain constant while out-of-plane fluctuations reflect stronger contraction during cooling. Above T_O, both in-plane and out-of-plane fluctuations follow temperature trends, indicating lattice stabilization due to oxygen reorganization. These observations underscore how structural anisotropy and lattice distortions are closely tied to superconductivity stabilization [70–74].

Since the superconducting properties of Cu1234 primarily originate from the CuO_2 planes, which are the central structural feature governing the transport properties of cuprate superconductors, we have characterized the Cu-O planar structure through the calculation of the in-plane strain. The strain is defined as $\varepsilon = 2 * 100 * (Cu{-}O_{eq} - Cu{-}O_{obs})/Cu{-}O_{eq}$, where $Cu{-}O_{eq} = 1.97$ Å represents the Cu-O bond distance in equilibrium conditions, as determined in Cu^{2+} ions in solution, and $Cu{-}O_{obs}$ is the observed bond distance Cu1-O1 in the basal plane, under our experimental conditions [65–67]. The factor of 100 is included to express the strain as a

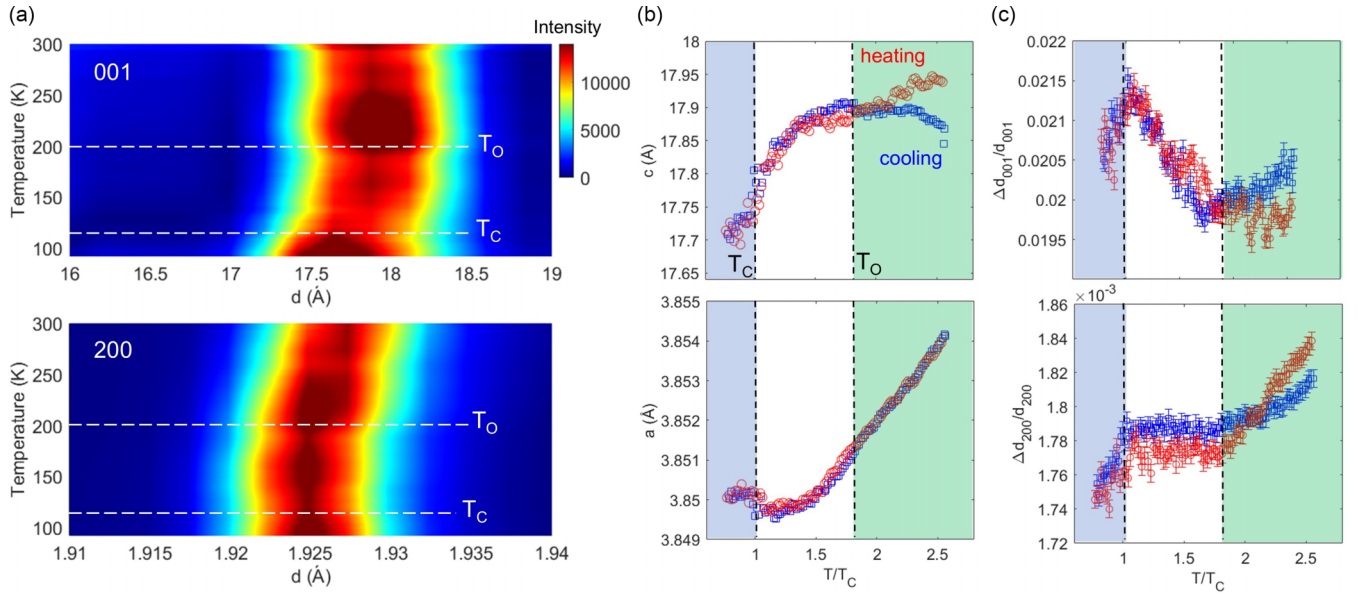

FIG. 2. (a) Colormaps of temperature dependence of 001 and 200 reflections. The superconducting and oxygen ordering temperatures T_C and T_O are indicated (white dashed lines). Temperature dependence of (b) unit cell parameters, c and a, and (c) fluctuations $\Delta d_{001}/d_{001}$ and (f) $\Delta d_{002}/d_{002}$. We observe a lattice anomaly at T_C where the *c*-axis sharply drops from 17.82 to 17.70 Å in the superconducting phase and the *a*-axis sharply increases from 3.8495 Å to 3.850 Å. The broadening of XRD peaks 001 and 200 at T_C, in panel (c) confirms the different regimes in the structural temperature evolution and the lattice anomaly at T_C.

percentage. We define a critical strain, $\varepsilon_c = 4.57\%$, corresponding to its value at the superconducting critical temperature T_C. Using this definition, a comprehensive phase diagram has been constructed (see Fig. 3), plotting the crystallographic axis ratio, c/a, and the normalized temperature as functions of the normalized strain $\varepsilon/\varepsilon_c$.

Here, we can see the distinct regimes previously described and indicated by colored areas, linked to the interplay between superconductivity and structural evolution. In the superconducting regime $T < T_C$ and $\varepsilon < \varepsilon_C$ (light blue area), the CuO_2 planar structure undergoes a stabilization process, reflecting the reduction in strain. Additionally, a metastable phase is identified for $\varepsilon > \varepsilon_c$ during cooling below $T_m = 165$ K, as highlighted in the orange-shaded region in Fig. 3. This phase likely arises from localized structural instabilities within the perovskite Cu-O planar bonds, reflecting their critical role in lattice dynamics in high T_c superconductivity.

In Fig. 4, we show the Cu(1)-O(1) bond distances derived from Rietveld refinement of synchrotron x-ray diffraction data collected using an incident wavelength of 0.7 Å. Due to limitations in angular resolution imposed by the PILATUS 2000 detector (pixel size: 172 × 172 μm²), the refined Cu(1)-O(1) bond distance exhibited larger fluctuations in comparison with Cu(1)-O(1) distances obtained through direct fitting of the (200) Bragg reflection, where the Cu(1)-O(1) distance corresponds to half the *a*-axis lattice parameter. This lower-energy dataset yielded smoother trends thanks to improved low-angle resolution, although it exhibited less distinct variations in its temperature-driven evolution, as shown in the previous Fig. 3. Anyway, the convergence of both methods underscores the robustness of the observed structural evolution.

Conversely, in the regime $T > T_O$ and $\varepsilon < \varepsilon_O$, (green area), where $\varepsilon_O = 4.49\%$ corresponds to the strain at $T = T_O$, structural fluctuations become irreversible, as shown in Fig. 2(b) by the *c*-axis temperature evolution. We report the Debye-Waller factors, U_{iso}, of oxygen atoms (see Fig. 5) to complement our analysis of geometrical fluctuations via Bragg reflection widths described in Fig. 2. We have analyzed the temperature-dependent behavior of U_{iso} at distinct oxygen sites. We have observed that $U_{iso}(O2)$, $U_{iso}(O3)$, and $U_{iso}(O4)$ exhibit a drop below T_C, indicating reduced atomic displacements and supporting the stabilization of the superconducting state. Between T_C and $T_O > 200$ K, $U_{iso}(O2)$ and $U_{iso}(O3)$ remain nearly constant, while $U_{iso}(O4)$ follows the temperature evolution. Above T_O, all three U_{iso} values increase upon heating and decrease upon cooling, closely mirroring *c*-axis trends and revealing irreversible reorganization of oxygen motion [see Fig. 2(b)]. Meanwhile, $U_{iso}(O1)$ remains consistently high and temperature-independent, pointing to persistent larger positional disorder. These findings look to indicate T_O as a temperature for oxygen diffusion in line with phenomena observed in other cuprate superconductors [42–46]. In particular, thermal treatment has shown the onset of interstitial oxygen rearrangement at temperatures larger than 200 K in La_2CuO_{4+y} [45].

Standard BCS single-gap theory does not predict lattice rearrangements at T_C. In Cu1234, however, the described sharp *c*-axis contraction of 0.12 Å (from 17.82 Å to 17.70 Å) and negative in-plane thermal expansion below T_C, represent anomalies beyond the scope of conventional BCS behavior. We interpret this as evidence for multigap superconductivity, arising from the heterostructure's layered architecture comprising metallic $[Ba_2CuO_{4-\gamma}]$ and Mott insulating $[Ca_3Cu_4O_8]$ planes, which foster charge disproportionation and multiband effects supported by multiple Fermi surfaces, measured by ARPES experiments in Hg-based cuprates [76–78]. Such anomalies may also reflect significant chemical potential shifts near the 3D–2D electronic

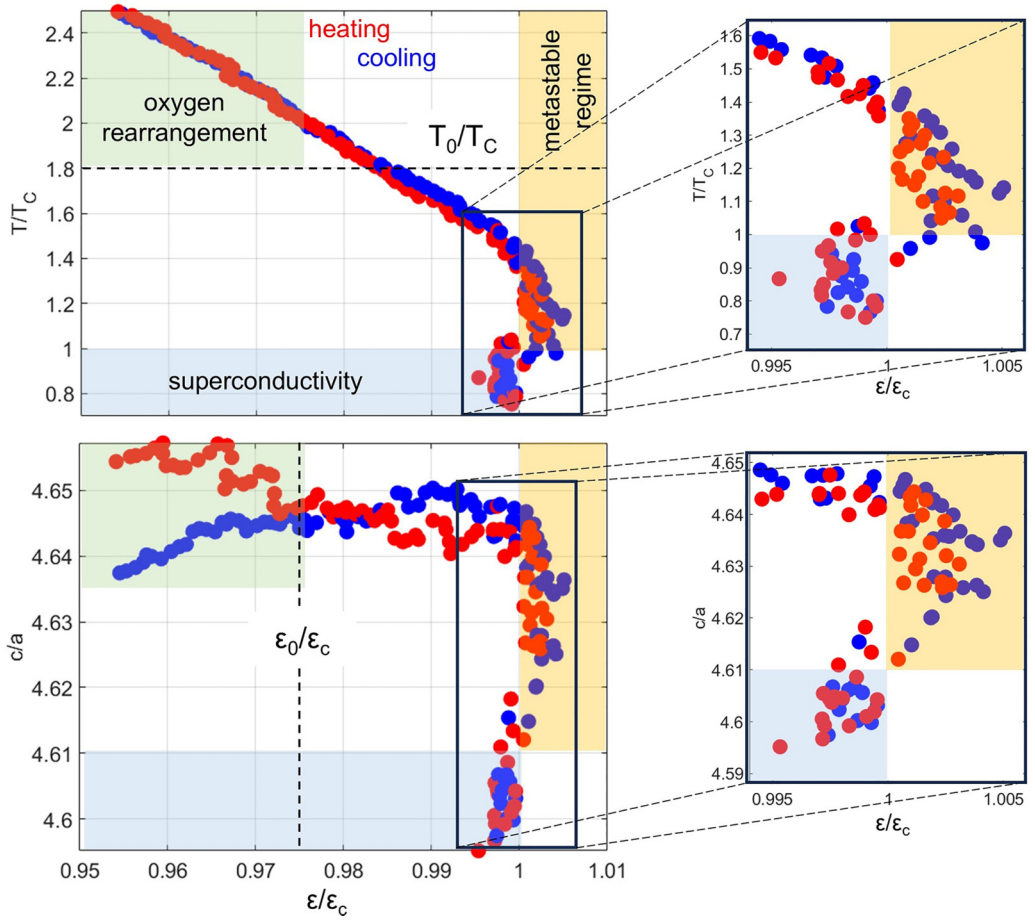

FIG. 3. (upper panel) Normalized temperature, T/T_C, and axis ratio, c/a, as a function of normalized strain, $\varepsilon/\varepsilon_c$. The superconducting phase (light blue area) occurs for $T < T_C$ and $\varepsilon < \varepsilon_c$ where $T_C = 118$ K and $\varepsilon_c = 4.57\%$. The oxygen rearrangement occurs for $T > T_O$ and $\varepsilon < \varepsilon_O$. When $T > T_C$ and $\varepsilon > \varepsilon_c$ the system undergoes a metastable phase (yellow area). Finally, for $\varepsilon < \varepsilon_c$ and $T > T_C$ we observe a decreasing strain. The structural phase transition at T_C is highlighted in the magnified panels on the right.

topological transition, where multiband shape resonances [32] amplify superconducting gap interactions across distinct bands. These combined factors support the proposed multigap superconductivity scenario, offering a more consistent explanation than a single-gap scenario.

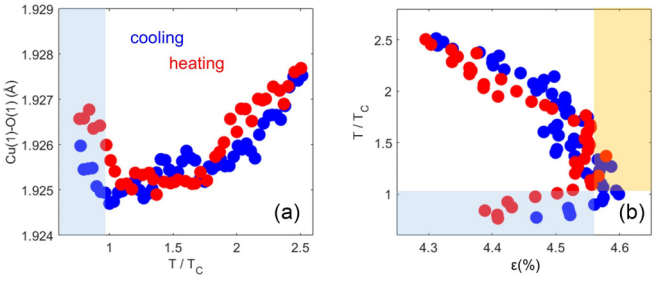

FIG. 4. (a) Cu(1)-O(1) bond distances derived from Rietveld refinement of synchrotron x-ray diffraction data collected at incident wavelengths of 0.6999 Å during cooling (blue circles) and heating (red circles) thermal ramps. (b) Normalized temperature, T/T_C, as a function of strain, ε. The light blue areas indicate the superconducting state, while the orange zones are associated with the metastable phase.

We have integrated our experimental findings for Cu1234 and the AHTS heterostructures [80] into the general "T_C-strain-doping" phase diagram of cuprates [64], as shown in Fig. 6. The Cu1234 superconductor, characterized by a strain $\varepsilon = 4.3\%$ at room temperature, doping $\delta = 0.29$, and the high T_C of 118 K [19], aligns with the strain-doping landscape of cuprates. Indeed, although this system resides in the overdoped regime, its strain leads it in proximity to the top of the superconducting dome for all families of standard hole-doped cuprate perovskites. In contrast, the artificial high T_c superlattices (AHTS) composed of La-based cuprates alternating dopants Sr-rich units and stoichiometric CuO_2 units exhibit a higher compressive strain $\varepsilon = 9\%$ and a significantly lower T_C of 43 K [65]. The elevated strain in MIMI shifts the system away from the ($\varepsilon_C \approx 0.04$ for $\delta_C = 0.16$), suppressing T_C. Thus, our Cu1234 system shows how strain engineering provides a pathway to optimize superconductivity at ambient pressure in cuprate perovskites.

Conversely, the MIMI structure underscores the lower superconductivity under larger strain. This duality emphasizes the need to balance doping and strain to engineer high-performance superconductors. The lattice anomaly associated with the superconducting transition provides key insights into the behavior of cuprates, particularly in the context of the

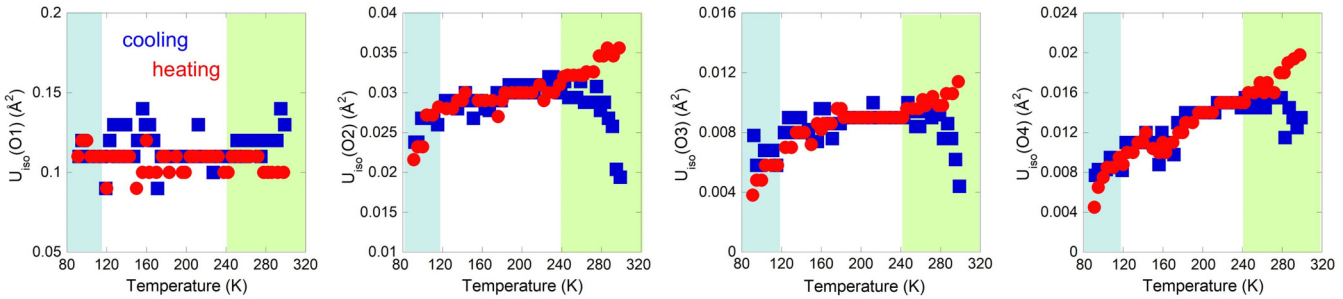

FIG. 5. Debye-Waller factors extracted from Rietveld refinement for oxygen in O1, O2, O3, and O4 sites. The light blue areas indicate the superconducting state, while the light green zones are associated with the oxygen diffusion temperature range.

resonant multigap superconductivity with relevant electron-lattice interaction [81–87]. In Cu1234, the lattice anomaly observed at the superconducting critical temperature is generated by the variation of the chemical potential as occurs in systems with multiple different gaps opening at T_c with a charge redistribution due to relevant electron-lattice interactions tuned by strain, identified as a critical factor [66–68]. Specifically, the interplay between lattice distortions and electronic properties in Cu1234 is evident in two key phenomena below T_C: the expansion of the CuO_2 planes and the compression of the interlayer spacing along the *c*-axis. These structural adjustments point to a strong coupling between electrons and phonons in hot spots of the electronic k-space, as well as multiband superconductivity. This interplay is tuned by strain favoring anisotropic lattice distortions due to chemical potential changes at the opening of multiple superconducting gaps.

III. CONCLUSIONS

Synchrotron x-ray diffraction measurements of Cu1234 reveal significant insights into the interplay between lattice geometry and superconductivity in this strongly overdoped high-temperature cuprate. The structure of Cu1234 can be classified as a layered MIMI structure. This architecture, comprised of alternating hole-doped Mott insulator $[Ca_3Cu_4O_8]$ units and metallic $[Ba_2CuO_{2+\delta}]$ layers, is crucial to its unique properties. The temperature-dependent analysis of the unit cell parameters, ***a*** and ***c***, and the in-plane strain, unveils distinct structural changes at the superconducting critical temperature, $T_C \sim 118$ K. Specifically, we observe anisotropic thermal expansion below T_C, with a negative thermal expansion along the ***a***-axis coupled with a contraction along the ***c***-axis. Furthermore, fluctuations in the d-spacings $\Delta d_{001}/d_{001}$ and $\Delta d_{200}/d_{200}$ and oxygen Debye-Waller factors exhibit clear differences across the different temperature regimes distinguished by superconducting and oxygen diffusion temperatures T_C and T_O, akin to observations in several cuprate high-temperature superconductors. Analyzing the in-plane *strain*, derived from the Cu-O basic planar structure, we construct a phase diagram correlating normalized temperature (T/T_C) and axis ratio (c/a) as a function of normalized strain ($\varepsilon/\varepsilon_c$). This diagram identifies a clear structural transition between $0.8 < T/T_c < 1.3$ with a compression of the *c*-axis and a sharp expansion of the *a*-axis at T_C with a decreasing strain, which is maximum around $T/T_c \approx 1.3$. The observed lattice anomaly at T_c is intrinsically linked to the opening of multiple superconducting gaps. Furthermore, the compressed local Cu1 octahedron indicates that the charge introduced by doping is localized on the strongly overdoped $[Ba_2CuO_{4-y}]$ layers. This charge localization provides a nanoscale electronic phase separation, within is likely a key factor in the enhancement of superconducting properties. The metallic $[Ba_2CuO_{4-y}]$ layers (of thickness $W = 4.33$ Å) play the role of overdoped metallic units, while the $[Ca_3Cu_4O_8]$ blocks (of thickness $L = 13.25$ Å) host the confined superconducting interface space charge, forming a MIMI. The nanoscale high T_c superlattice of quantum wells with period $d = 1.758$ nm is characterized by the geometry ratio $L/d = 0.75$ positioned near the top of the superconducting dome observed in artificial MIMI systems [81–86]. The Cu1234 structure achieves optimal strain-doping synergy, enabling its high $T_C \sim 118$ K. This natural MIMI configuration creates distinct CuO_2 planes: chemically overdoped metallic layers and chemically undoped layers. This underscores a fundamental departure from conventional cuprate models, where CuO_6 compressed local octahedron and heavily overdoped hole carriers [91–96] redefine the interplay between charge disproportionation and orbital hybridization, leading to multigap high-T_c superconducting mechanisms observed

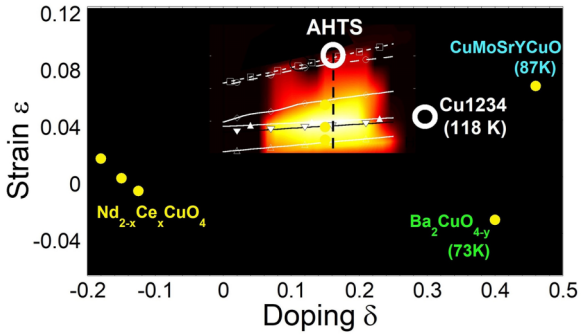

FIG. 6. General phase diagram for different cuprate perovskite families as a colormap of T_C (from $T_c = 0$ K, black, to $T_c \sim 135$ K, through yellow to white) as a function of strain, ε, and doping, δ [64,65]. Small open white symbols represent hole-doped cuprates. Maximum T_C occurs at $\delta = 0.16$ and $\varepsilon = 4\%$. The yellow full circles represent the electron-doped and highly overdoped cuprates [1–10,89–96]. The thick white empty circles indicate the Cu1234 sample with average doping $\delta = 0.29$ and strain 4% studied in this work, compared with the La-based AHTS with $T_C = 43$ K [81–86].

in artificial high-T_C superlattices [81–86]. The resulting charge and lattice phase separation as predicted by Jarlborg *et al.* [77–80] confined in Cu1234 by XANES spectroscopy [19] drives an emergent quantum electronic phase with nanoscale quantum size effects, proximity to a Lifshitz electronic topological transition in the presence of spin-orbit coupling at the interface. Such interfacial heterogeneity enhances quantum coherence in interface superconductivity in the stoichiometric units, a mechanism predicted by the BPV theory and verified experimentally in artificial high-T_C superlattices [81–86].

By integrating these findings into the universal "T_C-doping-strain" phase diagram, shown in Fig. 4, where we observe that the high average $p = 0.29$ hole/Cu site doping and the strain $\varepsilon = 4.2\%$ places Cu1234 at the optimal strain for the T_C maximum [66].

Our results highlight the importance of nanoscale phase separation [49–53,97–100] and the geometry of nanoscale structural complexity in governing the superconducting properties of Cu1234. Like in AHTS [29–33,81–87,101], where high T_c is controlled by the optimal lattice strain and geometry ratio $0.6 < L/d < 0.75$ in the special case where the metal units are heavily overdoped copper-oxide planes. Finally, our crystallographic and lattice distortion analyses offer a solid experimental foundation for characterizing the structural evolution of Cu1234 across the superconducting transition, which was observed previously in other cuprates [36] using a fast and local structure probe of complex matter x-ray spectroscopy with synchrotron radiation [63–65,102].

IV. METHODS

The x-ray diffraction (XRD) measurements for the powdered Cu1234 sample were conducted on the XRD1 beamline at the ELETTRA synchrotron radiation facility, Trieste, employing high-resolution transmission geometry [88]. Data acquisition spanned two thermal cycles, each consisting of a cooling ramp followed by a heating ramp. In the first thermal cycle, measurements were performed using a photon wavelength of 0.7 Å, which provided higher resolution and was therefore employed for structural Rietveld refinement analysis. During the second cycle, a wavelength of 1.4809 Å was used, optimized for studying the temperature evolution of structural parameters through more precise fitting of the 001 and 200 reflections. The Pilatus2M detector was positioned 86 mm from the sample. The sample temperature was systematically varied between 90 K and 300 K. At each temperature set point, the system was allowed to equilibrate until the temperature gradient within the sample was less than 0.1 K, ensuring reliable measurements. All acquired diffraction images were processed using the FIT2D software suite. Structural analyses were performed using the Expo2 Rietveld refinement program [89], while additional temperature-dependent parameter evaluations were conducted with custom MATLAB routines developed in-house.

ACKNOWLEDGMENTS

We thank the Superstripes ONLUS and the CNR project DCM.AD006.562 "Functional Disorder in Materials and Complex Systems" for supporting this work. We thank the Institute of Physics, Chinese Academy of Sciences (IOPACS) for financial support.

DATA AVAILABILITY

The data that support the findings of this article are available from the authors upon reasonable request.

[1] M. Marezio, O. Chmaissem, C. Bougerol, M. Karppinen, H. Yamauchi, and T. H. Geballe, Overdoped cuprates with high-temperature superconducting transitions, APL Mater. **1**, 021103 (2013).

[2] S. D. Conradson, T. H. Geballe, C. Q. Jin, L.-P. Cao, A. Gauzzi, M. Karppinen, G. Baldinozzi, W.-M. Li, E. Gilioli, J. M. Jiang, M. Latimer, O. Mueller, and V. Nasretdinova, Nonadiabatic coupling of the dynamical structure to the superconductivity in $YSr_2Cu_{2.75}Mo_{0.2}O_{7.54}$ and $Sr_2CuO_{3.3}$, Proc. Natl. Acad. Sci. USA **117**, 33099 (2020).

[3] S. D. Conradson, T. H. Geballe, A. Gauzzi, M. Karppinen, C. Jin, G. Baldinozzi, W. Li, L. Cao, E. Gilioli, Jack M. Jiang, M.Latimer, O. Mueller, and V. Nasretdinova, Local lattice distortions and dynamics in extremely overdoped superconducting $YSr_2Cu_{2.75}$ $Mo_{0.25}O_{7.54}$, Proc. Natl. Acad. Sci. USA **117**, 4559 (2020).

[4] O. Chmaissem, I. Grigoraviciute, H. Yamauchi, M. Karppinen, and M. Marezio, Superconductivity and oxygen ordering correlations in the homologous series of $(Cu, Mo)Sr_2(Ce, Y)_sCu_2O_{5+2s+\delta}$, Phys. Rev. B **82**, 104507 (2010).

[5] A. Gauzzi, Y. Klein, M. Nisula, M. Karppinen, P. K. Biswas, H. Saadaoui, E. Morenzoni, P. Manuel, D. Khalyavin, M. Marezio, and T. H. Geballe, Bulk superconductivity at 84 K in the strongly overdoped regime of cuprates, Phys. Rev. B **94**, 180509(R) (2016).

[6] S. D. Conradson, T. H. Geballe, C. Jin, L. Cao, G. Baldinozzi J.M. Jiang, M. J. Latimer, and O. Mueller, Local structure of $Sr_2CuO_{3.3}$, a 95 K cuprate superconductor without CuO_2 planes, Proc. Natl. Acad. Sci. USA **117**, 4565 (2020).

[7] W. M. Li, J. F. Zhao, L. P. Cao, Z. Hu, Q. Z. Huang, X. C. Wang, R. Z. Yu, Y. W. Long, H. Wu, H. J. Lin, C. T. Chen, Z. Z. Gong, Z. Guguchia, J. S. Kim, G. R. Stewart, Y. J. Uemura, S. Uchida, and C. Q. Jin, The Unconventional copper oxide superconductor with conventional constitution, J. Supercond. Nov. Magn. **33**, 81 (2020).

[8] L. Sederholm, S. D. Conradson, T. H. Geballe, C.-Q. Jin, A. Gauzzi, E. Gilioli, M. Karppinen, and G. Baldinozzi, Extremely overdoped superconducting cuprates via high pressure oxygenation methods, Condens. Matter **6**, 50 (2021).

[9] P. Adhikary, M. Gupta, A. Chauhan, S. Satpathy, S. Mukherjee, and B. R. K. Nanda, Unique d_{xy} superconducting state in the cuprate, Phys. Rev. B **109**, L020505 (2024).

[10] W. M. Li, J. F. Zhao, L. P. Cao, Z. Hu, Q. Z. Huang, X. C. Wang, Y. Liu, G. Q. Zhao, J. Zhang, Q. Q. Liu, R. Z. Yu, Y. W. Long, H. Wu, H. J. Lin, C. T. Chen, Z. Li, Z. Z. Gong,

Z. Guguchia, J. S. Kim, G. R. Stewart, Y. J. Uemura, S. Uchida, and C. Q. Jin, Superconductivity in a unique type of copper oxide, Proc. Natl. Acad. Sci. USA **116**, 12156 (2019).

[11] E. V. Antipov, S. M. Loureiro, C. Chaillout, J. J. Capponi, P. Bordet, J. L. Tholence, S. N. Putilin, and M. Marezio, The synthesis and characterization of the $HgBa_2Ca_2Cu_3O_{8+\delta}$ and $HgBa_2Ca_3Cu_4O_{10+\delta}$ phases, Physica C **215**, 1 (1993).

[12] S. Taku, K. Shimizu, H. Eisaki, A. Iyo, and S. Uchida, High-pressure effect on T_c of $HgBa_2Ca_3Cu_4O_{10+\delta}$ up to 30 GPa, J. Phys. Conf. Ser. **121**, 052009 (2008).

[13] R. V. Lutciv and Y. V. Boyko, Extra oxygen and carrier distribution in CuO_2 layers in $HgBa_2Ca_{n-1}CunO_{2n+2+\delta}$ compounds (n = 1, 2, 4), Condens. Matter Phys. **2**, 481 (1999).

[14] G. A. Bordovskii, A. V. Marchenko, F. S. Nasredinov, and P. P. Seregin, Charge states of atoms in ceramic superconductors $HgBa_2Ca_{n-1}Cu_nO_{2n+2}$, $Tl_2Ba_2Ca_{n-1}Cu_nO_{2n+4}$ and $Bi_2Sr_2Ca_{n-1}CunO_{2n+4}$ (n = 1 3), Glas. Phys. Chem. **36**, 411 (2010).

[15] C. Q. Jin, S. Adachi, X. J. Wu, H. Yamauchi, and S. Tanaka, 117 K superconductivity in the Ba–Ca–Cu–O system, Physica C **223**, 238 (1994).

[16] C. Q. Jin, S. Adachi, X.-J. Wu, and H. Yamauchi, *A New Superconducting Homologous Series of Compounds: Cu-12(n-1)n:P, Advances in Superconductivity* (Springer-Verlag, Tokyo, 1995), pp. 249–254.

[17] C.-J. Liu, C.-Q. Jin, and H. Yamauchi, Thermoelectric power of high pressure synthesized $CuBa_2Ca_3Cu_4O_{11-\delta}$, Phys. Rev. B **53**, 5170 (1996).

[18] J. F. Zhao, W. M. Li, and C. Q. Jin, Composition simple and environmental friendly high temperature cuprate superconductors: Cu12(*n*-1)*n*, Sci. China Phys. Mech. Astron. **48**, 087405 (2018).

[19] X. Zhang, J. Zhao, H. Zhao, L. Shi, S. Deng, J. Chen, L. He, Z. Hu, C. Jin, and J. Zhu, Atomic origin of the coexistence of high critical current density and high T_c in $CuBa_2Ca_3Cu_4O_{10+\delta}$ superconductors, NPG Asia Mater. **14**, 50 (2022).

[20] A. Lynnyk, R. Puzniak, L. Shi, J. Zhao, and C. Jin, Superconducting state properties of $CuBa_2Ca_3Cu_4O_{10+\delta}$, Materials **16**, 5111 (2023).

[21] C. Q. Jin, X. M. Qin, K. Shimizu, M. Nishiyama, T. Namiki, and Y. Yu, The enhanced superconductivity of Cu-1234 under high pressure, Int. J. Mod. Phys. B **19**, 335 (2005).

[22] D. Larbalestier, Critical currents and magnet applications of high-Tc superconductors, Phys. Today **44**(6), 74 (1991).

[23] S. Graser, P. J. Hirschfeld, T. Kopp, R. Gutser, B. M. Andersen, and J. Mannhart, How grain boundaries limit supercurrents in high-temperature superconductors, Nat. Phys. **6**, 609 (2010).

[24] X.-J. Wu, S. Adachi, C.-Q. Jin, H. Yamauchi, and S. Tanaka, Novel homologous series of superconducting copper oxides, Cu-12(*n*-1)*n*, Physica C **223**, 243 (1994).

[25] K. Tanaka, W. S. Lee, D. H. Lu, A. Fujimori, T. Fujii, Risdiana, I. Terasaki, D. J. Scalapino, T. P. Devereaux, Z. Hussain, and Z.-X. Shen, Distinct Fermi-momentum-dependent energy gaps in deeply underdoped Bi2212, Science **314**, 1910 (2006).

[26] T. Yoshida, M. Hashimoto, S. Ideta, A. Fujimori, K. Tanaka, N. Mannella, Z. Hussain, Z.-X. Shen, M. Kubota, K. Ono, S. Komiya, Y.Ando, H. Eisaki, and S. Uchida, Universal versus material-dependent two-gap behaviors of the high-T_c cuprate superconductors: Angle-resolved photoemission study of $La_{2-x}Sr_xCuO_4$, Phys. Rev. Lett. **103**, 037004 (2009).

[27] D. Mihailovic, and K. A. Müller, *The Two-Component Paradigm for Superconductivity in the Cuprates in High-T_c Superconductivity 1996: Ten Years after the Discovery* (Springer Netherlands, Dordrecht, 1997), pp. 243–256.

[28] N. Barišić and D. K. Sunko, High-Tc cuprates: A story of two electronic subsystems, J. Supercond. Nov. Magn. **35**, 1781 (2022).

[29] A. Bianconi, On the possibility of new high T_c superconductors by producing metal heterostructures as in the cuprate perovskites, Solid State Commun. **89**, 933 (1994).

[30] A. Bianconi, Feshbach shape resonance in multiband superconductivity in heterostructures, J. Supercond. **18**, 625 (2005).

[31] A. Bianconi, Multiband superconductivity in high T_c cuprates and diborides, J. Phys. Chem. Solids **67**, 567 (2006).

[32] D. Innocenti, N. Poccia, A. Ricci, A. Valletta, S. Caprara, A. Perali, and A. Bianconi, Resonant and crossover phenomena in a multiband superconductor: Tuning the chemical potential near a band edge, Phys. Rev. B—Cond. Matter Mater. Phys. **82**, 184528 (2010).

[33] A. Bussmann-Holder, H. Keller, A. Simon, and A. Bianconi, Multi-band superconductivity and the steep band/flat band scenario, Condens. Matter **4**, 91 (2019).

[34] H. Tajima, H. Aoki, A. Perali, and A. Bianconi, Emergent Fano-Feshbach resonance in two-band superconductors with an incipient quasiflat band: Enhanced critical temperature evading particle-hole fluctuations, Phys. Rev. B **109**, L140504 (2024).

[35] A. Bianconi, Shape resonances in multi-condensate granular superconductors formed by networks of nanoscale-striped puddles, J. Phys. Conf. Ser. **449**, 012002 (2013).

[36] M. Acosta-Alejandro, J. M. Mustre de León, S. D. Conradson, and A. R. Bishop, Evidence for a local structural change in $La_2CuO_{4.1}$ across the superconducting transition, J. Supercond. **15**, 355 (2002).

[37] S. Ideta, K. Takashima, M. Hashimoto, T. Yoshida, A. Fujimori, H. Anzai, T. Fujita, Y. Nakashima, A. Ino, M. Arita, H. Namatamem M. Taniguchi, K. Ono, M. Kubota, D. H. Lu, Z.-X. Shen, K. M. Kojima, and S. Uchida, Enhanced superconducting gaps in the trilayer high-temperature $Bi_2Sr_2Ca_2Cu_3O_{10+\delta}$ cuprate superconductor, Phys. Rev. Lett. **104**, 227001 (2010).

[38] T. Yoshida, W. Malaeb, S. Ideta, D. H. Lu, R. G. Moor, Z. X. Shen, and A. Fujimori, Coexistence of a pseudogap and a superconducting gap for the high-T_c superconductor $La_{2-x}Sr_xCuO_4$ studied by angle-resolved photoemission spectroscopy, Phys. Rev. B **93**, 014513 (2016).

[39] R. Sekine, S. Nakayama, A. Tsukada, S. J. Denholme, N. Miyakawa, and K. Tokiwa, Different electronic states at crystallographically inequivalent CuO_2 planes on four-layered cuprates $HgBa_2Ca_3Cu_4O_{10+\delta}$, J. Phys. Conf. Ser. **969**, 012031 (2018).

[40] C. Wen, Z. Hou, A. Akbari, K. Chen, W. Hong, H. Yang, I. Eremin, Y. Li, and H.-H. Wen, Unprecedentedly large gap in $HgBa_2Ca_2Cu_3O_{8+\delta}$ with the highest T_c at ambient pressure, npj Quantum Mater. **10**, 20 (2025).

[41] A. Ricci, N. Poccia, B. Joseph, L. Barba, G. Arrighetti, G. Ciasca, J.-Q. Ya, R. W. McCallum, T. A. Lograsso, N. D. Zhigadlo, J. Karpinski, and A. Bianconi, Structural phase

transition and superlattice misfit strain of *R*FeAsO (R = La, Pr, Nd, Sm), Phys. Rev. B **82**, 144507 (2010).

[42] G. Campi, A. Ricci, N. Poccia, L. Barba, G. Arrighetti, M. Burghammer, A. S. Caporale, and A. Bianconi, Scanning micro-x-ray diffraction unveils the distribution of oxygen chain nanoscale puddles in $YBa_2Cu_3O_{6.33}$, Phys. Rev. B **87**, 014517 (2013).

[43] M. V. Zimmermann, J. R. Schneider, T. Frello, N. H. Andersen, J. Madsen, M. Käll, H. F. Poulsen, R. Liang, P. Dosanjh, and W. N. Hardy, Oxygen-ordering superstructures in underdoped $YBa_2Cu_3O_{6+x}$ studied by hard x-ray diffraction, Phys. Rev. B **68**, 104515 (2003).

[44] M. Fratini, N. Poccia, A. Ricci, G. Campi, M. Burghammer, G. Aeppli, and A. Bianconi, Scale-free structural organization of oxygen interstitials in La_2CuO_{4+y}, Nature (London) **466**, 841 (2010).

[45] N. Poccia, M. Fratini, A. Ricci, G. Campi, L. Barba, A. Vittorini-Orgeas, G. Bianconi, G. Aeppli, and A. Bianconi, Evolution and control of oxygen order in a cuprate superconductor, Nat. Mater. **10**, 733 (2011).

[46] G. Campi, A. Bianconi, N. Poccia, G. Bianconi, L. Barba, G. Arrighetti, D. Innocenti, J. Karpinski, N. D. Zhigadlo, S. M. Kazakov, M. Burghammer, M. v. Zimmermann, M. Sprung, and A. Ricci, Inhomogeneity of charge-density-wave order and quenched disorder in a high-T_c superconductor, Nature (London) **525**, 359 (2015).

[47] J. G. Bednorz, and K. A. Müller, *Earlier and Recent Aspects of Superconductivity: Lectures from the International School, Erice, Trapani, Sicily, July 4-16, 1989 (Vol. 90)* (Springer, Berlin, Heidelberg, 1990).

[48] K. A. Müller, The first five years of high-T_c superconductivity, Physica C **185**, 3 (1991).

[49] E. Sigmund and K. A. Müller, *Phase separation in cuprate superconductors: Proceedings of the Second International Workshop on "Phase Separation in Cuprate Superconductors"* (Springer Science Business Media, Berlin, Heidelberg, 2012).

[50] K. A. Müller and A. Bussmann-Holder, *Superconductivity in Complex Systems* (Springer Science Business Media, Berlin, Heidelberg, 2005).

[51] K. A. Müller, From phase separation to stripes, in *Stripes and Related Phenomena* (Springer US, Boston, MA, 2000), pp. 1–8.

[52] K. A. Müller, The unique properties of superconductivity in cuprates, J. Supercond. Nov. Magn. **27**, 2163 (2014).

[53] *Proceedings of the Workshop on Phase Separation in Cuprate Superconductors: Erice, Italy, 6-12 May 1992*, edited by K. A. Muller and G. Benedek (World Scientific, Singapore, 1993).

[54] A. Shengelaya, H. Keller, K. A. Müller, B. I. Kochelaev, and K. Conder, Tilting mode relaxation in the electron paramagnetic resonance of oxygen-isotope-substituted $La_{2-x}Sr_xCuO_4$: Mn^{2+}, Phys. Rev. B **63**, 144513 (2001).

[55] K. A. Müller, Electron paramagnetic resonance and high temperature superconductivity, J. Supercond. Nov. Magn. **19**, 53 (2006).

[56] J. S. Zhou, G. I. Bersuker, and J. B. Goodenough, Nonadiabatic electron-lattice interactions in the copper-oxide superconductors, J. Supercond. **8**, 541 (1995).

[57] T. Egami, Alex and the origin of high-temperature superconductivity, in *High-T_c Copper Oxide Superconductors and Related Novel Materials*, edited by A. Bussmann-Holder, H. Keller, and A. Bianconi (Springer, Cham, 2017).

[58] J. B. Goodenough, and J.-S. Zhou, New forms of phase segregation, Nature (London) **386**, 229 (1997).

[59] J. S. Zhou and J. B. Goodenough, Electron-lattice coupling and stripe formation in $La_{2-x}Ba_xCuO_4$, Phys. Rev. B **56**, 6288 (1997).

[60] J. B. Goodenough, J. S. Zhou, and G. I. Bersuker, Thermoelectric Power and normal state of the high-T_c copper oxides in *Anharmonic Properties of High-T_c Cuprates-Proceedings of the International Workshop* (World Scientific, Singapore, 1995).

[61] J. B. Goodenough, Ordering of bond length fluctuations in the copper-oxide superconductors, Europhys. Lett. **57**, 550 (2002).

[62] J. B. Goodenough, and F. Rivadulla, Bond-length fluctuations in transition-metal oxides, Mod. Phys. Lett. B **19**, 1057 (2005).

[63] A. P. Menushenkov, A. V. Kuznetsov, R. V. Chernikov, A. A. Ivanov, V. V. Sidorov, and K. V. Klementiev, Low temperature anharmonicity and superconductivity in cuprates, J. Supercond. Nov. Magn. **27**, 925 (2014).

[64] A. Menushenkov, A. Kuznetsov, R. Chernikov, A. Ivanov, V. Sidorov, and K. Klementiev, Correlation of the local and the macroscopic properties of high-temperature superconductors, Z. Kristallogr. Cryst. Mater. **225**, 487 (2010).

[65] A. Bianconi, N. L. Saini, A. Lanzara, M. Missori, T. Rossetti, H. Oyanagi, H. Yamaguchi, K. Oka, and T. Ito, Determination of the local lattice distortions in the CuO_2 plane of $La_{1.85}Sr_{0.15}CuO_4$, Phys. Rev. Lett. **76**, 3412 (1996).

[66] A. Bianconi, G. Bianconi, S. Caprara, D. D. Castro, H. Oyanagi, and N. L. Saini, The stripe critical point for cuprates, J. Phys. Condens. Matter **12**, 10655 (2000).

[67] S. Agrestini, D. D. Castro, M. Sansone, N. L. Saini, A. Bianconi, A. Saccone, S. De NegriI, M. Giovannini, and M. Colapietro, Anisotropic thermal expansion in diborides as a function of micro-strain, Int. J. Mod. Phys. B **17**, 812 (2003).

[68] M. Fratini, R. Caivano, A. Puri, A. Ricci, Z.-A. Ren, X.-Li Dong, J. Yang, Wei Lu, Z.-X. Zhao, L. Barba, G. Arrighetti, M. Polentarutti, and A. Bianconi, The effect of internal pressure on the tetragonal to monoclinic structural phase transition in ReOFeAs: The case of NdOFeAs, Supercond. Sci. Technol. **21**, 092002 (2008).

[69] P. Fornasini, G. Dalba, R. Grisenti, J. Purans, M. Vaccari, F. Rocca, and A. Sanson, Local behaviour of negative thermal expansion materials, Nucl. Instrum. Methods Phys. Res. B **246**, 180 (2006).

[70] J. Purans, N. D. Afify, G. Dalba, R. Grisenti, S. De Panfilis, A. Kuzmin, V. I. Ozhogin, F. Rocca, A. Sanson, S. I. Tiutiunnikov, and P. Fornasini, Isotopic effect in extended x-ray-absorption fine structure of germanium, Phys. Rev. Lett. **100**, 055901 (2008).

[71] J. Timoshenko, A. Kuzmin, and J. Purans, EXAFS study of hydrogen intercalation into ReO_3 using the evolutionary algorithm, J. Phys. Condens. Matter **26**, 055401 (2014).

[72] J. Purans, P. Fornasini, S. E. Ali, G. Dalba, A. Kuzmin, and F. Rocca, X-ray absorption spectroscopy study of local dynamics and thermal expansion in ReO_3, Phys. Rev. B **92**, 014302 (2015).

[73] J. Purans, S. Piskunov, D. Bocharov, A. Kalinko, A. Kuzmin, S. E. Ali, and F. Rocca, Local structure of perovskites ReO_3 and ScF_3 with negative thermal expansion: Interpretation beyond the quasiharmonic approximation, J. Phys. Conf. Ser. **712**, 012013 (2016).

[74] D. Bocharov, M. Krack, Y. Rafalskij, A. Kuzmin, and J. Purans, Ab initio molecular dynamics simulations of negative thermal expansion in ScF_3: The effect of the supercell size, Comput. Mater. Sci. **171**, 109198 (2020).

[75] V. Palmisano, S. Agrestini, G. Campi, M. Filippi, L. Simonelli, M. Fratini, A. Bianconi, S. De Negri, M. Giovannini, A. Saccone, A. N. Fitch, M. Brunelli, and I. Margiolaki, Anomalous thermal expansion in superconducting $Mg_{1-x}Al_xB_2$ system, J. Supercond. **18**, 737 (2005).

[76] L. Barba, G. Chita, G. Campi, L. Suber, E. M. Bauer, A. Marcelli, and A. Bianconi, Anisotropic thermal expansion of p-terphenyl: a self-assembled supramolecular array of poly-*p*-phenyl nanoribbons, J. Supercond. Nov. Magn. **31**, 703 (2018).

[77] T. Jarlborg and A. Bianconi, Fermi surface reconstruction of superoxygenated La_2CuO_4 superconductors with ordered oxygen interstitials, Phys. Rev. B **87**, 054514 (2013).

[78] T. Jarlborg and A. Bianconi, Electronic structure of $HgBa_2CuO_{4+\delta}$ with self-organized interstitial oxygen wires in the Hg spacer planes, J. Supercond. Novel Magn. **31**, 689 (2018).

[79] A. R. Bishop, A lattice litany for transition metal oxides, Condensed Matter **5**, 46 (2020).

[80] G. Campi, M. V. Mazziotti, T. Jarlborg, and A. Bianconi, Scale-free distribution of oxygen interstitial wires in optimum-doped $HgBa_2CuO_{4+y}$, Condensed Matter **7**, 56 (2022).

[81] A. Bianconi, High Tc superconductors made by metal heterostructures at the atomic limit, European Patent EP0733271A1 (1998), https://patents.google.com/patent/EP0733271A1/en.

[82] M. V. Mazziotti, A. Bianconi, R. Raimondi, G. Campi, and A. Valletta, Spin–orbit coupling controlling the superconducting dome of artificial superlattices of quantum wells, J. Appl. Phys. **132**, 193908 (2022).

[83] G. Logvenov, N. Bonmassar, G. Christiani, G. Campi, A. Valletta, and A. Bianconi, The superconducting dome in artificial high-T_c superlattices tuned at the Fano–Feshbach resonance by quantum design, Condens. Matter **8**, 78 (2023).

[84] G. Campi, G. Logvenov, S. Caprara, A. Valletta, and A. Bianconi, Kondo versus Fano in superconducting artificial high-T_c heterostructures, Condens. Matter **9**, 43 (2024).

[85] A. Valletta, A. Bianconi, A. Perali, G. Logvenov, and G. Campi, High-T_c superconducting dome in artificial heterostructures made of nanoscale quantum building blocks, Phys. Rev. B **110**, 184510 (2024).

[86] H. G. Ahmad, D. Massarottti, F. Tafuri, G. Logvenov, A. Bianconi, and G. Campi, Josephson coupling in lanthanum-based cuprate superlattices, APL Quantum **2**, 016113 (2025).

[87] G. Campi, A. Alimenti, G. Logvenov, G. A. Smith, F. F. Balakirev, S.-E. Lee, L. Balicas, E. Silva, G. A. Ummarino, G. Midei, A. Perali, A. Valletta, and A. Bianconi, Upper critical magnetic field and multiband superconductivity in artificial high-T_c superlattices of nano quantum wells, Phys. Rev. Mater. **9**, 074204 (2025).

[88] A. Lausi, M. Polentarutti, S. Onesti, J. R. Plaisier, E. Busetto, G. Bais, L. Barba, A. Cassetta, G. Campi, D. Lamba, A. Pifferi, S. C. Mande, D. D. Sarma, S. M. Sharma, and G. Paolucci, Status of the crystallography beamlines at Elettra, Eur. Phys. J. Plus **130**, 43 (2015).

[89] A. Altomare, C. Cuocci, C. Giacovazzo, A. Moliterni, R. Rizzi, N. Corriero, and A. Falcicchio, *EXPO2013*: a kit of tools for phasing crystal structures from powder data, J. Appl. Crystallogr. **46**, 1231 (2013).

[90] W. M. Li, L. P. Cao, J. F. Zhao, X. C. Wang, R. Z. Yu, Y. W. Long, Q. Q. Liu, and C. Q. Jin, Superconductivity of a cuprate with compressed local octahedron, Sci. China Phys. Mech. Astron. **62**, 037421 (2019).

[91] K. Jiang, C. Le, Y. Li, S. Qin, Z. Wang, F. Zhang, and J. Hu, Electronic structure and two-band superconductivity in unconventional high-T_c cuprates $Ba_2CuO_{3+\delta}$, Phys. Rev. B **103**, 045108 (2021).

[92] Hyo Sun Jin, W. E. Pickett, and K. W. Lee, Two-band conduction and nesting instabilities in superconducting $Ba_2CuO_{3+\delta}$: First-principles study, Phys. Rev. B **104**, 054516 (2021).

[93] X. C. Bai, Y. M. Quan, H. Q. Lin, and L. J. Zou, Band crossover and magnetic phase diagram of the high-T_c superconducting compound $Ba_2CuO_{4-\delta}$, Phys. Rev. B **105**, 184506 (2022).

[94] M. Zegrodnik, P. Wójcik, and J. Spałek, Superconducting dome with extended *s*-wave pairing symmetry in the heavily hole-overdoped copper-oxide planes, Phys. Rev. B **103**, 144511 (2021).

[95] P. Worm, M. Kitatani, J. M. Tomczak, L. Si, and K. Held, Hidden one-dimensional, strongly nested, and almost half-filled Fermi surface in Ba_2CuO_{3+y} superconductors, Phys. Rev. B **105**, 085110 (2022).

[96] A. Hemmatzade, E. Medina, L. Delbes, B. Baptiste, D. Hrabovsky, Y. Klein, S. D. Conradson, M. Karppinen, and A. Gauzzi, T_c saturation and possible electronic phase separation in strongly overdoped cuprates, Condensed Matter **8**, 5 (2023).

[97] K. I. Kugel, A. L. Rakhmanov, and A. O. Sboychakov, Phase separation in Jahn-Teller systems with localized and itinerant electrons, Phys. Rev. Lett. **95**, 267210 (2005).

[98] K. I. Kugel, A. L. Rakhmanov, A. O. Sboychakov, and D. I. Khomskii, Doped orbitally ordered systems: Another case of phase separation, Phys. Rev. B–Condens. Matter Mater. Phys. **78**, 155113 (2008).

[99] K. I. Kugel, A. L. Rakhmanov, and A. O. Sboychakov, Electronic phase separation in magnetic materials, Phys. Met. Metall. **123**, 674 (2022).

[100] M. Y. Kagan, K. I. Kugel, A. L. Rakhmanov, and A. O. Sboychakov, Electronic phase separation in magnetic and superconducting materials: recent advances, in *Springer Series in Solid-State Sciences*, Vol. 201 (Springer, Cham, 2024), p. 379.

[101] J. Y. Shen, C. Y. Shi, Z. M. Pan, L. L. Ju, M. D. Dong, G. F. Chen, Y. C. Zhang, J. K. Yuan, C. J. Wu, Y. W. Xie, and J. Wu, Reentrance of interface superconductivity in a high-T_c cuprate heterostructure, Nat. Commun. **14**, 7290 (2023).

[102] A. Bianconi, S. Doniach, and D. Lublin, X-ray Ca K edge of calcium adenosine triphosphate system and of simple Ca compounds, Chem. Phys. Lett. **59**, 121 (1978).